Effects of shear and rotation on the spherical collapse model for clustering dark energy

Francesco Pace,[1][⋆] Ronaldo C. Batista[2] and Antonino Del Popolo[3,4]

[1]*Institute for Cosmology and Gravitation, University of Portsmouth, Dennis Sciama Building, Portsmouth PO1 3FX, UK*
[2]*Escola de Ciências e Tecnologia, Universidade Federal do Rio Grande do Norte Caixa Postal 1524, 59072-970 Natal, Rio Grande do Norte, Brazil*
[3]*Dipartimento di Fisica e Astronomia, University Of Catania, Viale Andrea Doria 6, I-95125 Catania, Italy*
[4]*International Institute of Physics, Universidade Federal do Rio Grande do Norte, 59012-970 Natal, Brazil*

ABSTRACT

In the framework of the spherical collapse model, we study the influence of shear and rotation terms for dark matter fluid in clustering dark energy models. We evaluate, for different equations of state, the effects of these terms on the linear overdensity threshold parameter, δ_c, and on the virial overdensity, Δ_V. The evaluation of their effects on δ_c allows us to infer the modifications occurring on the mass function. Due to ambiguities in the definition of the halo mass in the case of clustering dark energy, we consider two different situations: the first is the classical one where the mass is of the dark matter halo only, while the second one is given by the sum of the mass of dark matter and dark energy. As previously found, the spherical collapse model becomes mass dependent and the two additional terms oppose the collapse of the perturbations, especially on galactic scales, with respect to the spherical non-rotating model, while on cluster scales the effects of shear and rotation become negligible. The values for δ_c and Δ_V are higher than the standard spherical model. Regarding the effects of the additional non-linear terms on the mass function, we evaluate the number density of haloes. As expected, major differences appear at high masses and redshifts. In particular, quintessence (phantom) models predict more (less) objects with respect to the Λ colddarkmatter model, and the mass correction due to the contribution of the dark energy component has negligible effects on the overall number of structures.

Key words: methods: analytical – cosmology: theory – dark energy.

1 INTRODUCTION

One of the most complex puzzle in modern cosmology is the understanding of the nature of the accelerated expansion of the Universe. This astonishing fact is the result of observations of high-redshifts supernovae, which are less luminous of what was expected in a decelerated universe (Riess et al. 1998; Perlmutter et al. 1999; Tonry et al. 2003). Assuming general relativity and interpreting the dimming of Type Ia supernovae (SNIa) as due to an accelerated expansion phase in the history of the Universe, we are forced to introduce a new component with negative pressure, and in particular, to cause accelerated expansion, its equation-of-state parameter must be $w < -1/3$. This fluid, usually dubbed *dark energy* (DE), is totally unknown in its nature and physical characteristics.

The latest observations of SNIa (Riess et al. 1998, 2004, 2007; Perlmutter et al. 1999; Knop et al. 2003; Astier et al. 2006; Amanullah et al. 2010), together with the cosmic microwave background (CMB; Jarosik et al. 2011; Komatsu et al. 2011; Planck Collabo-

ration 2013a,b,c; Sievers et al. 2013), the integrated Sachs–Wolfe effect (Giannantonio et al. 2008; Ho et al. 2008), the large scale structure (LSS) and baryonic acoustic oscillations (Tegmark et al. 2004a,b; Cole et al. 2005; Eisenstein et al. 2005; Percival et al. 2010; Reid et al. 2010; Blake et al. 2011), the globular clusters (Krauss & Chaboyer 2003; Dotter, Sarajedini & Anderson 2011), high-redshift galaxies (Alcaniz, Lima & Cunha 2003) and the galaxy clusters (Haiman, Mohr & Holder 2001; Allen et al. 2004, 2008; Wang et al. 2004; Basilakos, Plionis & Solà 2010), till works based on weak gravitational lensing (Hoekstra et al. 2006; Jarvis et al. 2006) and X-ray clusters (Vikhlinin et al. 2009) confirmed these early findings and they are all in agreement with a universe filled with 30 per cent by cold dark matter (CDM) and baryons (both fluids pressureless) and with the remaining 70 per cent by the cosmological constant Λ (the so-called ΛCDM model). The cosmological constant is the most basic form of DE. Its equation of state is constant in time ($w = -1$), it appears in Einstein field equations as a geometrical term, it cannot cluster (being constant in space and time) and its importance is appreciable only at low redshift.

Despite being in agreement virtually with all the observables, the standard cosmological model suffers from severe theoretical

[⋆] E-mail: francesco.pace@port.ac.uk

problems (the coincidence and the fine-tuning problems), and therefore alternative models have been explored (but see also Astashenok & del Popolo 2012). The most studied ones are minimally coupled scalar fields (quintessence models). Since gravity is the main interaction acting on large scales, it is commonly believed that structures in the Universe formed via gravitational instability of primordial overdense perturbations that originated in the primeval inflationary phase (Starobinsky 1980; Guth 1981; Linde 1990) of the Universe from quantum, Gaussian distributed fluctuations (Del Popolo 2007, 2014; Komatsu 2010; Casaponsa et al. 2011; Curto et al. 2011; Komatsu et al. 2011; Hinshaw et al. 2013).

Differently from the cosmological constant, even if often neglected in the literature, dynamical DE models possess fluctuations that can alter the evolution of structure formation, not only via slowing down the growth rate but also giving rise to DE overdensities and underdensities which can evolve into the non-linear regime.

To study structure formation in the highly non-linear regime, it is very useful to work within the framework of the spherical collapse model (SCM), introduced by Gunn & Gott (1972) and extended in many following works (Fillmore & Goldreich 1984; Bertschinger 1985; Hoffman & Shaham 1985; Ryden & Gunn 1987; Avila-Reese, Firmani & Hernández 1998; Subramanian, Cen & Ostriker 2000; Ascasibar et al. 2004; Mota & van de Bruck 2004; Williams, Babul & Dalcanton 2004; Abramo et al. 2007; Pace, Waizmann & Bartelmann 2010; Pace et al. 2014). According to the model, perturbations are considered as being spherically symmetric non-rotating objects that, being overdense, decouple from the background Hubble expansion, reach a point of maximum expansion (turnaround) and collapse (formally to a singularity). In reality, this does not happen and the kinetic energy associated with the collapse is converted into random motions creating an equilibrium configuration (a virialized structure).

Despite its crude approximations, the model is very successful in reproducing results of *N*-body simulations when mass is combined with the function formalism (Del Popolo 2007; Hiotelis & del Popolo 2013), either in usual minimally coupled DE models (Pace et al. 2010) or in non-minimally coupled DE models (Pace et al. 2014). Nevertheless, it is important to extend the basic formalism to include additional terms and make it more realistic.

Consequences of relaxing the sphericity assumption were studied by Hoffman (1986, 1989) and Zaroubi & Hoffman (1993), while the introduction of radial motions and angular momentum was deeply studied by Ryden & Gunn (1987) and Gurevich & Zybin (1988a,b). We refer to Del Popolo, Pace & Lima (2013c) for a more complete list of references and for details on the different models and how to link the angular momentum to the matter overdensity.

In this work, we will extend previous works on the extended spherical collapse model (ESCM) in DE models (Del Popolo, Pace & Lima 2013a; Del Popolo et al. 2013b,c) by taking into account perturbations of the DE fluid. Since there are no *N*-body simulations with clustering DE so far, such study is valuable in order to have an idea about how DE fluctuations impact structure formation in a more realistic scenario. By writing the differential equations describing the dynamics of dark matter (DM) and DE, we will show how to relate the additional terms (shear and angular momentum) to the overdensity field and we will solve them to derive the time evolution of the typical parameters of the SCM, in particular the linear overdensity threshold for collapse δ_c and the virial overdensity Δ_V, and we will show how these quantities are modified by the introduction of non-zero vorticity and shear terms. Afterwards we will show how the mass function and its phenomenological extension to include DE perturbations are affected.

This paper is organized as following. In Section 2, we discuss and summarize the DE models used in this work. In Section 3, we briefly derive the equations of the ESCM whose solution will lead to the evaluation of δ_c and Δ_V (see Section 4.1). In Section 4, we show our results and in particular, we devote Section 4.2 to the discussion of the effects of shear and rotation on the mass function. Finally, we conclude in Section 5.

2 THE MODELS

For this work, we use DE models previously analysed in the framework of the SCM where the usual assumption of negligible DE fluctuations is relaxed.

DE models, described by an equation of state $w = P/(\rho c^2)$, either constant or time dependent, satisfy the background continuity equation

$$\dot{\rho} + 3H(1 + w)\rho = 0 . \tag{1}$$

We consider eight different models and for the ones characterized by an evolving equation-of-state parameter, we adopt the Chevallier & Polarski (2001) and Linder (2003) (CPL) linear parameterization

$$w(a) = w_0 + (1 - a)w_a , \tag{2}$$

where w_0 and w_a are constants and a is the scale factor.

The reference model is the standard ΛCDM model where DE is represented by the cosmological constant with equation-of-state parameter $w = -1$, constant along the whole cosmic history. A consequence of this parameterization is that at early times this model behaves essentially as the Einstein–de Sitter (EdS) model (with $\Omega_m = 1$ and $\Omega_{de} = 0$), and the influence of the cosmological constant becomes appreciable only late in the cosmic history.

Due to the latest observational results by the *Planck* satellite[1] (Planck Collaboration 2013a,b,d), we will assume a spatially flat model.

Of the remaining seven models, two have a constant equation-of-state parameter $w > -1$ (the quintessence models DE1 and DE2) and they differ from each other solely for the exact value of w. Other two instead have $w < -1$ (the phantom models DE3 and DE4). The latter are justified by recent SNIa observations (Novosyadlyj et al. 2012; Planck Collaboration 2013b; Rest et al. 2013; Scolnic et al. 2013; Shafer & Huterer 2014).

Finally, we consider three additional models with a time-varying equation of state. Once again we can distinguish them according to the general behaviour of the equation-of-state parameter. One model enters in the quintessence model category (DE5), the second one is a phantom model (DE6) and the last one (DE7) is characterized by the barrier crossing, i.e. the model considered shows a phantom regime at low redshifts ($w < -1$) and a quintessence regime at earlier times ($w > -1$).

As previously stated, quintessence models are described by a scalar field not interacting with matter and are fully described by a kinetic and a potential energy term. Since the nature of DE is unknown, the potential has an ad hoc functional form and its second derivative represents the mass of the scalar field. These models naturally have an evolving DE equation of state w. Scalar fields are therefore viable candidates for the DE component.

Phantom models instead have $w < -1$ and challenge the foundations of theoretical physics violating several energy conditions. Phantom models have a negative defined kinetic energy term and

[1] http://sci.esa.int/planck/

Table 1. Values of the parameters describing the equations of state considered in this work.

Model	w_0	w_a
ΛCDM	-1	0
DE1	-0.9	0
DE2	-0.8	0
DE3	-1.1	0
DE4	-1.2	0
DE5	-0.75	0.4
DE6	-1.1	-1.0
DE7	-1.1	0.5
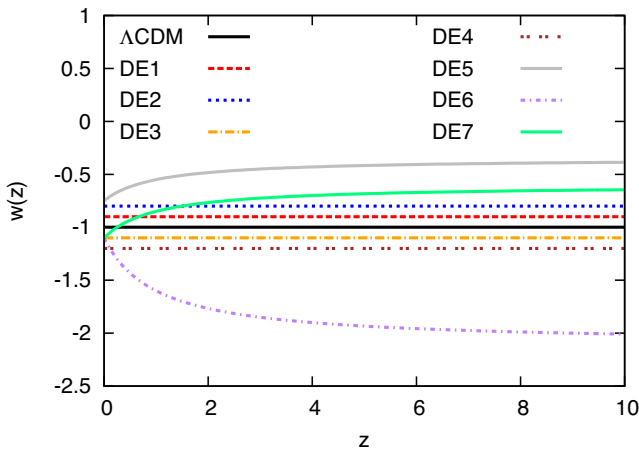
Figure 1. Time evolution of the equation-of-state parameter as a function of the redshift z for the DE models studied in this work. The black, red, blue, orange and brown lines represent the ΛCDM, the DE1, the DE2, the DE3 and the DE4 model, respectively. The grey line represents the DE5 model, the purple line the DE6 model and the green line the DE7 model.

due to the super-negative equation of state, the energy budget of the Universe gets completely dominated by them in the future.

The solution of equation (1) is (for a generic time-dependent equation-of-state parameter $w(a)$)

$$\rho(a) = \rho(a=1)e^{-3\int_1^a [1+w(a')]\mathrm{d}\ln a'} . \tag{3}$$

In the particular case of constant equation of state, equation (3) reduces to

$$\rho(a) = \rho(a=1)a^{-3(1+w)} , \tag{4}$$

where it appears clearly that for the cosmological constant $\rho(a) = \rho(a=1)$, and hence the name.

In this work, we will use the following cosmological parameters (recall that the curvature is null): $\Omega_{\mathrm{m}} = 0.32$ and $\Omega_{\mathrm{de}} = 0.68$, while $h = 0.72$, in agreement with recent determinations by *Planck* (Planck Collaboration 2013b) for flat ΛCDM models. The normalization of the power spectrum for the ΛCDM model is $\sigma_8 = 0.776$.

In Table 1, we give the values of the parameters describing the equations of state of the models considered here both for a null time evolution (models DEn, with n from 1 to 4) and for a time evolution (models DEn, with n from 5 to 7) of the equation of state. We recall that for $w_a = 0$, the CPL parametrization reduces to a constant equation of state with $w = w_0$. We show the time evolution of the equation-of-state parameter $w(z)$ in Fig. 1. For models DEn, with $n = 5, 6, 7$, the variation of the equation of state as a function of

the redshift is quite mild, with major variations for $z \lesssim 2$. At higher redshifts, all the three models reach a constant value for the equation of state, being $w = -0.35, -2, -0.6$ for models DE5, DE6, DE7, respectively. We also point out that the barrier crossing for model DE7 takes place for $z \approx 0.25$, having a phantom (quintessence) behaviour for smaller (higher) redshifts. We checked that all the models do not have an appreciable amount of DE at early times; therefore, they cannot be considered as belonging to the class of early DE models.

Perturbations for DE are described by the effective sound speed c_{eff}^2 that relates density perturbations to pressure perturbations via the relation $\delta p = c_{\mathrm{eff}}^2 \delta \rho c^2$. In the following, we will consider two different values for the effective sound speed, usually assumed in the literature: $c_{\mathrm{eff}}^2 = 0$ (clustering DE) and $c_{\mathrm{eff}}^2 = 1$ (smooth DE). Canonical scalar fields have $c_{\mathrm{eff}}^2 = 1$, whereas models with vanishing c_{eff}^2 can be built from k-essence models (Armendariz-Picon, Mukhanov & Steinhardt 2001; Chimento & Lazkoz 2005; Creminelli et al. 2009) or two scalar fields (Lim, Sawicki & Vikman 2010). We will show in Section 3 how this term enters into the equations for the (extended) SCM.

3 EXTENDED SPHERICAL COLLAPSE MODEL

In this section, we review the basic formalism used to derive the equations for the SCM and how this can be extended to include shear and rotation terms.

The basic assumption in the framework of the SCM is that objects form under the gravitational collapse of spherical DM overdense perturbations. This is clearly a rather crude assumption because it is known that primordial seeds are not spherical, but they are triaxial and rotate (see e.g. Bardeen et al. 1986; Del Popolo, Ercan & Xia 2001; Del Popolo 2002; Shaw et al. 2006; Bett et al. 2007). Nevertheless, the model accurately reproduces the results of *N*-body simulations.

The spherical and ellipsoidal collapse models were extensively investigated in the literature (see e.g. Bardeen et al. 1986; Bernardeau 1994; Ohta, Kayo & Taruya 2003, 2004; Basilakos, Sanchez & Perivolaropoulos 2009; Basilakos et al. 2010; Pace et al. 2010) assuming that DE perturbations are negligible, while other studies took into account also the effects of perturbations for the DE fluid (see Mota & van de Bruck 2004; Nunes & Mota 2006; Abramo et al. 2007, 2008, 2009b; Abramo, Batista & Rosenfeld 2009a; Creminelli et al. 2010; Basse, Eggers Bjælde & Wong 2011; Batista & Pace 2013). More recently, the SCM was extended to investigate coupled (Pettorino & Baccigalupi 2008; Wintergerst & Pettorino 2010; Tarrant et al. 2012) and extended DE (scalar–tensor) models (Pettorino & Baccigalupi 2008; Pace et al. 2014).

While the general equations including the shear and rotation were explicitly written in the case of smooth DE (Pace et al. 2010) and for clustering DE (Abramo et al. 2007), the effects of these two non-linear terms were investigated only recently in Del Popolo et al. (2013a,c) for smooth DE models and in Del Popolo et al. (2013b) for Chaplygin cosmologies.

Following Abramo et al. (2007, 2008), the full perturbed equations describing the evolution of the dark matter (δ_{DM}) and dark energy (δ_{DE}) perturbations are

$$\delta_{\mathrm{DM}}' + (1 + \delta_{\mathrm{DM}})\frac{\theta_{\mathrm{DM}}}{aH} = 0 , \tag{5}$$

$$\delta_{\mathrm{DE}}' - \frac{3}{a}w\delta_{\mathrm{DE}} + [1 + w + \delta_{\mathrm{DE}}]\frac{\theta_{\mathrm{DE}}}{aH} = 0 . \tag{6}$$

In the previous equations, w represents the equation of state of DE at the background level and the prime is the derivative with respect to the scale factor. The two variables θ_{DM} and θ_{DE} are the divergence of the peculiar velocity for the dark matter and the dark energy component, respectively. Equation (6) is valid in the limit $c_{eff}^2 = 0$, the limit of clustering DE. For the case $c_{eff}^2 > 0$, DE perturbations are usually negligible on small scales, as shown for example in Batista & Pace (2013).

To determine the equation for the evolution of the divergence of the peculiar velocity, we have to make some assumptions on the influence of the shear and rotation terms on the perturbations of the two fluids considered. If we assume that only DM experiences shear and rotation terms, then the two peculiar velocities are different ($\theta_{DM} \neq \theta_{DE}$) and we will have two different equations: one including shear and rotation for the DM and one for the DE component without the extra terms. If instead we assume that DE experiences the effects of the shear and the rotation terms in the same fashion of the DM component, then the two peculiar velocities will be the same and we need to solve a single differential equation.

Here, we explicitly write the two different equations for the peculiar velocities and in the next sections, we will study the consequences of this assumption. Having therefore two different Euler equations, the equations for the divergence of the peculiar velocities are

$$\theta_{DM}' + \frac{2}{a}\theta_{DM} + \frac{\theta_{DM}^2}{3aH} + \frac{\sigma_{DM}^2 - \omega_{DM}^2}{aH}$$
$$+ \frac{3H}{2a}[\Omega_{DM}\delta_{DM} + \Omega_{DE}\delta_{DE}] = 0, \tag{7}$$

$$\theta_{DE}' + \frac{2}{a}\theta_{DE} + \frac{\theta_{DE}^2}{3aH} + \frac{3H}{2a}[\Omega_{DM}\delta_{DM} + \Omega_{DE}\delta_{DE}] = 0 . \tag{8}$$

The shear tensor σ_{ij} and the vorticity tensor ω_{ij} are defined as

$$\sigma_{ij} = \frac{1}{2}\left(\frac{\partial u^j}{\partial x^i} + \frac{\partial u^i}{\partial x^j}\right) - \frac{1}{3}\theta\delta_{ij} , \tag{9}$$

$$\omega_{ij} = \frac{1}{2}\left(\frac{\partial u^j}{\partial x^i} - \frac{\partial u^i}{\partial x^j}\right) . \tag{10}$$

The terms σ^2 and ω^2 represent the contractions of the tensors σ_{ij} and ω_{ij}, respectively.

It is convenient to consider a dimensionless divergence of the comoving peculiar velocity, defined as $\tilde{\theta} = \theta/H$. Therefore, equations (5)–(8) read now

$$\delta_{DM}' + (1 + \delta_{DM})\frac{\tilde{\theta}_{DM}}{a} = 0 , \tag{11}$$

$$\delta_{DE}' - \frac{3}{a}w\delta_{DE} + [1 + w + \delta_{DE}]\frac{\tilde{\theta}_{DE}}{a} = 0 , \tag{12}$$

$$\tilde{\theta}_{DM}' + \left(\frac{2}{a} + \frac{H'}{H}\right)\tilde{\theta}_{DM} + \frac{\tilde{\theta}_{DM}^2}{3a}$$
$$+ \frac{\tilde{\sigma}_{DM}^2 - \tilde{\omega}_{DM}^2}{a} + \frac{3}{2a}[\Omega_{DM}\delta_{DM} + \Omega_{DE}\delta_{DE}] = 0, \tag{13}$$

$$\tilde{\theta}_{DE}' + \left(\frac{2}{a} + \frac{H'}{H}\right)\tilde{\theta}_{DE} + \frac{\tilde{\theta}_{DE}^2}{3a}$$
$$+ \frac{3}{2a}[\Omega_{DM}\delta_{DM} + \Omega_{DE}\delta_{DE}] = 0. \tag{14}$$

We remind the reader that this set of equations is valid when DE is not affected by shear and rotation, otherwise equations (13) and (14) will be identical and $\theta_{DM} = \theta_{DE}$.

To solve the system of equations (11)–(14), it is necessary to determine the initial conditions. At early times, the aforementioned system of equations can be linearized and it reads

$$\delta_{DM}' = -\frac{\tilde{\theta}_{DM}}{a} , \tag{15}$$

$$\delta_{DE}' - \frac{3}{a}w\delta_{DE} = -(1 + w)\frac{\tilde{\theta}_{DE}}{a} , \tag{16}$$

$$\tilde{\theta}_{DM}' + \left(\frac{2}{a} + \frac{H'}{H}\right)\tilde{\theta}_{DM} = -\frac{3}{2a}[\Omega_{DM}\delta_{DM} + \Omega_{DE}\delta_{DE}] , \tag{17}$$

$$\tilde{\theta}_{DE}' + \left(\frac{2}{a} + \frac{H'}{H}\right)\tilde{\theta}_{DE} = -\frac{3}{2a}[\Omega_{DM}\delta_{DM} + \Omega_{DE}\delta_{DE}] . \tag{18}$$

Hence at the linear level, the peculiar velocity perturbations are identical for both fluids.

The initial value for the DM overdensity can be found as outlined in Pace et al. (2010, 2012, 2014) and Batista & Pace (2013). Here we just recall the general procedure. Since at collapse time a_c the collapsing sphere reduces to a point, its density is formally infinite. Therefore, the initial overdensity $\delta_{DM,i}$ is given by the value such that $\delta_{DM} \to +\infty$ for $a \to a_c$. Knowing $\delta_{DM,i}$ and assuming that at early times it behaves as a power law, $\delta_{DM} = Aa^n$, it is easy to evaluate the initial amplitude for the DE and the peculiar velocity perturbations:

$$\delta_{DE,i} = \frac{n}{(n - 3w)}(1 + w)\delta_{DM,i} , \tag{19}$$

$$\tilde{\theta}_{DM,i} = -n\delta_{DM,i} . \tag{20}$$

$$\tilde{\theta}_{DE,i} = \tilde{\theta}_{DM,i} . \tag{21}$$

For an EdS model, $n = 1$, but in general, deviations for DE models are very small, even for early DE models (Ferreira & Joyce 1998; Batista & Pace 2013).

To evaluate the functional form of the term $\sigma_{DM}^2 - \omega_{DM}^2$, we refer to the works by Del Popolo et al. (2013a,c), and we define the quantity α as the ratio between the rotational and the gravitational term

$$\alpha = \frac{L^2}{M^3 RG} , \tag{22}$$

where M and R are the mass and the radius of the spherical overdensity, respectively, and L its angular momentum. Values for α range from 0.05 for galactic masses ($M \approx 10^{11}\, M_\odot\, h^{-1}$) to 3×10^{-6} for cluster scales ($M \approx 10^{15}\, M_\odot\, h^{-1}$).

As explained in Del Popolo et al. (2013c), the basic assumption made here is that the collapse preserves the value of the ratio of the acceleration between the shear rotation term and the gravitational field. This is a reasonable assumption as explained in Del Popolo et al. (2013c). As shown in Del Popolo et al. (2013b), based on the above-outlined argument for the definition of the rotation term, the additional term in the equations for the SCM (see equation 13) is

$$\tilde{\sigma}_{DM}^2 - \tilde{\omega}_{DM}^2 = -\frac{3}{2}\alpha\Omega_{DM}\delta_{DM} . \tag{23}$$

According to this ansatz, equation (13) now reads

$$\tilde{\theta}_{DM}' + \left(\frac{2}{a} + \frac{H'}{H}\right)\tilde{\theta}_{DM} + \frac{\tilde{\theta}_{DM}^2}{3a}$$
$$+ \frac{3}{2a}[(1 - \alpha)\Omega_{DM}\delta_{DM} + \Omega_{DE}\delta_{DE}] = 0. \tag{24}$$

If instead also DE is affected by shear and rotation, in the same way as DM, both velocity fields are determined by the equation

$$\tilde{\theta}' + \left(\frac{2}{a} + \frac{H'}{H} \right) \tilde{\theta} + \frac{\tilde{\theta}^2}{3a} + \frac{3}{2a}(1 - \alpha)\left[\Omega_{\mathrm{DM}} \delta_{\mathrm{DM}} + \Omega_{\mathrm{DE}} \delta_{\mathrm{DE}} \right] = 0 \; . \tag{25}$$

4 RESULTS

In this section, we present results for the linear and non-linear evolution of perturbations. We first start with quantities derived in the framework of the SCM and then continue with a discussion of how rotation and shear affect the mass function in clustering DE cosmologies.

As shown in Batista & Pace (2013), the main difficulty is to study the evolution of DE perturbations in the non-linear regime (see also Mota & van de Bruck 2004; Nunes & Mota 2006; Abramo et al. 2007; Creminelli et al. 2010; Basse et al. 2011).

Batista & Pace (2013) clearly demonstrated that DE fluctuations are very sensitive to the value of c_{eff}^2: when $c_{\mathrm{eff}}^2 = 1$, on small scales, where non-linear evolution is important, DE fluctuations are negligible with respect to the DM fluctuations δ_{DM}; therefore, ignoring them when solving the system of equations describing the ESCM (equations 11, 12, 14 and 24) does not introduce any significant error. Different is the situation when $c_{\mathrm{eff}}^2 = 0$, since DE fluctuations can be comparable to the DM ones. In this case, we cannot neglect them, otherwise the error introduced will be significant and invalidate our results and conclusions.

4.1 Parameters of the ESCM

The two main quantities that can be evaluated working within the framework of the ESCM are the linear overdensity parameter δ_{c} and the virial overdensity Δ_{V}. The linear overdensity parameter is a fundamental theoretical quantity entering, together with the linear growth factor, into analytical formulations of the mass function (see e.g. Press & Schechter 1974; Sheth, Mo & Tormen 2001; Sheth & Tormen 2002). The virial overdensity, instead, is used to define the size of haloes when considered spherical. Given a halo of mass M, it represents the mean density enclosed in the radius R and the mass and the radius are related to each other via the relation $M = 4/3\pi\bar{\rho}(z)\Delta_{\mathrm{V}}(z)R^3$, where $\bar{\rho}(z) = \bar{\rho}_{,0}(1 + z)^3$ is the mean matter density in the Universe.

Once the initial conditions are found, we can evolve equations (15)–(18) from the initial time $a_{\mathrm{i}} \approx 10^{-5}$ to the collapse time a_{c}. This function therefore depends on both the linear and non-linear evolution of perturbations.

In Fig. 2, we show the time evolution of the linear overdensity parameter δ_{c} for the usual case when shear and rotations are not included. We do so in order to better show how the additional terms modify this function. We show our results grouping the models as quintessence (top panel), phantom (middle panel) and barrier-crossing models (bottom panel). We refer to the caption for line styles and colours of each model.

The first important point to highlight is that quintessence models ($w \geq -1$) always show a lower $\delta_{\mathrm{c}}(z)$ with respect to the ΛCDM model, while the phantom models always have a higher value, due to the fastest accelerated expansion of the universe, which hinders structure formation. We also notice that models with $c_{\mathrm{eff}}^2 = 0$ are more similar to the ΛCDM model than for the case with $c_{\mathrm{eff}}^2 = 1$, in agreement with what was found by Batista & Pace (2013) for early DE models, where we refer for a deeper explanation. For
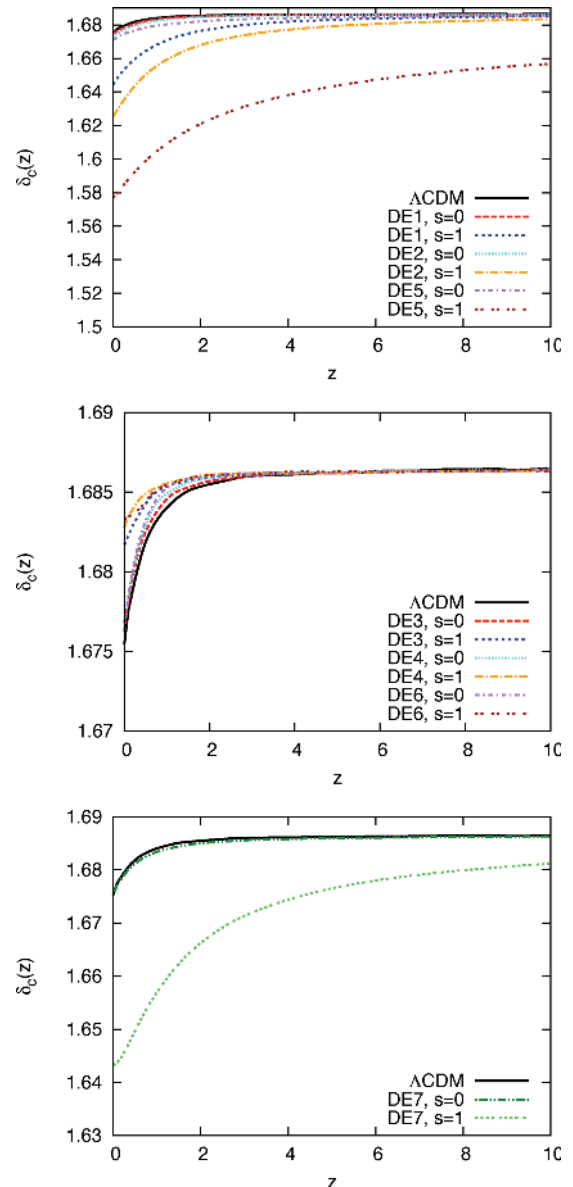
Figure 2. Linear overdensity parameter $\delta_{\mathrm{c}}(z)$ for quintessence (upper panel), phantom (middle panel) and models with barrier crossing (bottom panel). In the upper panel, model DE1 with $c_{\mathrm{eff}}^2 = 0$ ($c_{\mathrm{eff}}^2 = 1$) is shown with a dashed red (blue short dashed) curve, model DE2 with $c_{\mathrm{eff}}^2 = 0$ ($c_{\mathrm{eff}}^2 = 1$) is shown with cyan dotted (yellow dot–dashed) curve and model DE5 with $c_{\mathrm{eff}}^2 = 0$ ($c_{\mathrm{eff}}^2 = 1$) with a violet dotted short-dashed (brown dot-dotted) curve. In the middle panel, model DE3 with $c_{\mathrm{eff}}^2 = 0$ ($c_{\mathrm{eff}}^2 = 1$) is shown with a red dashed (blue short-dashed) curve, model DE4 with $c_{\mathrm{eff}}^2 = 0$ ($c_{\mathrm{eff}}^2 = 1$) is shown with a cyan dotted (yellow dot–dashed) curve while model DE6 with $c_{\mathrm{eff}}^2 = 0$ ($c_{\mathrm{eff}}^2 = 1$) is shown with violet dotted short-dashed (brown dot-dotted) curve. In the bottom panel, model DE7 with $c_{\mathrm{eff}}^2 = 0$ ($c_{\mathrm{eff}}^2 = 1$) is shown with a dark green dot-dotted short-dashed (light green dot-dot-dotted) curve. In all the panels, a solid black line shows the ΛCDM model. For simplicity, we used the notation $s = c_{\mathrm{eff}}^2$ in the labels.

our purposes, it suffices to recall that this happens because DE perturbations contribute to the gravitational potential via the Poisson equation. Model DE7 has a very similar behaviour to the other classes of models, in particular to the quintessence models. The linear overdensity parameter is smaller than the one for the ΛCDM model. When $c_{\mathrm{eff}}^2 = 0$, this model is almost identical to the ΛCDM model, while it differs substantially when $c_{\mathrm{eff}}^2 = 1$. All the models
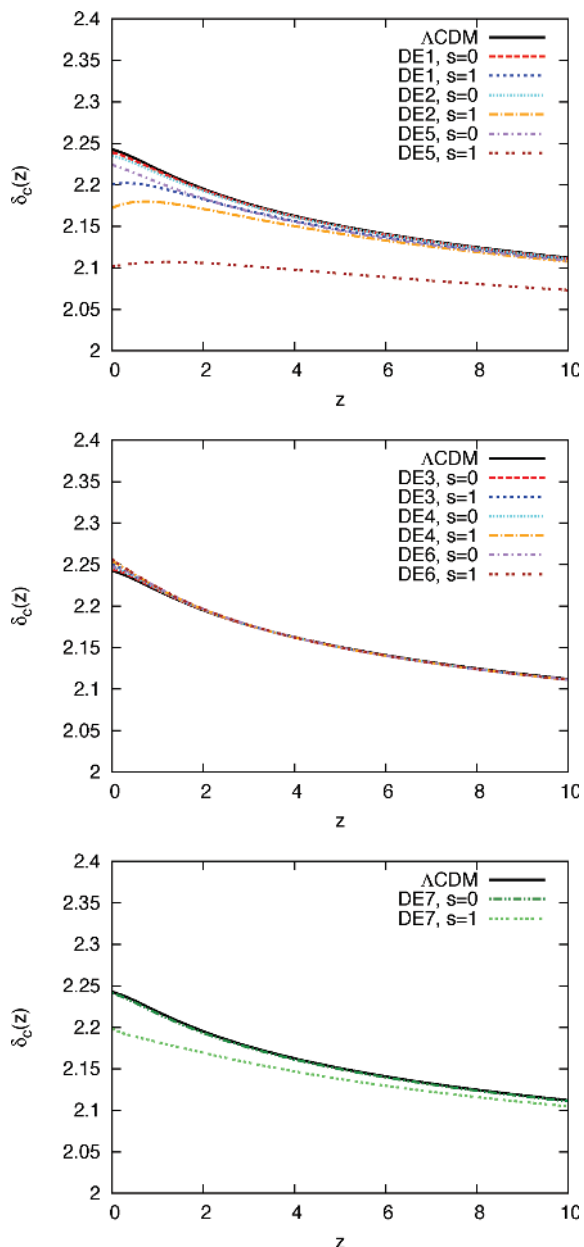
Figure 3. Linear overdensity parameter $\delta_c(z)$ for quintessence (upper panel), phantom (middle panel) and models with barrier crossing (bottom panel) including the shear and rotation terms in the equations for the evolution of the perturbations. Panels refer to galactic-scale mass objects ($M \approx 10^{11} \, \mathrm{M}_\odot \, h^{-1}$), corresponding to $\alpha = 0.05$. Line styles and colours are the same as in Fig. 2.

with effective sound speed $c_{\mathrm{eff}}^2 = 0$ converge very rapidly ($z \gtrsim 3$) to the ΛCDM model and hence to the EdS model, since DE becomes negligible at such high redshifts. Different again is the situation for the $c_{\mathrm{eff}}^2 = 1$ case, where the DE models recover the ΛCDM model at much higher redshifts (quintessence models), while phantom models reproduce the reference model very quickly. Models DE5 and DE7 with $c_{\mathrm{eff}}^2 = 1$ instead do not recover the ΛCDM model even at high redshifts. As said before, this is largely due to the additional source for the gravitational potential and largely independent of the background equation of state w, as shown in Pace et al. (2010).

In Fig. 3, we show results for δ_c when the shear and rotation terms are taken into account for the DM Euler equation. As already

shown and discussed in Del Popolo et al. (2013a,b,c), the main effect appears at galactic scales ($M \approx 10^{11} \, \mathrm{M}_\odot \, h^{-1}$). We verified that this is indeed the case also for clustering DE models; therefore, we will limit ourselves to present our results for galactic-scale objects. The differences between the SCM and the ESCM become increasingly smaller with increasing mass, disappearing at cluster scales. Qualitatively, therefore, clustering and non-clustering DE models behave in the same way with respect to the mass dependence. We refer to the caption for line styles and colours of each model.

As expected, and in analogy with the ESCM, when the influence of DE is only at the background level (Del Popolo et al. 2013c), the additional term opposes the collapse; therefore, the values for the linear overdensity parameter are higher than for the case in which these terms are neglected. Also in this case, quintessence models with $c_{\mathrm{eff}}^2 = 1$ differ more from the ΛCDM model than for the case with $c_{\mathrm{eff}}^2 = 0$. Phantom models are now very similar to the ΛCDM model, differently from before. Differences between the case with $c_{\mathrm{eff}}^2 = 0$ and 1 are now negligible. Model DE7 behaves qualitatively as for the standard SCM. Also in this case all the models, except for models DE5 and DE7 with $c_{\mathrm{eff}}^2 = 1$, recover the ΛCDM model at high redshifts. As shown in Del Popolo et al. (2013a,c), in the ESCM major differences take place at low redshifts. We can therefore conclude that clustering DE models behave similarly to the non-clustering DE models when shear and rotations are included in the analysis.

However, DE and its perturbations can also affect the virialization process of DM. A reference work focusing on this issue is Maor & Lahav (2005). In this seminal work, it was shown that a different result for the ratio between the virialization radius and the turnaround radius (the radius of maximum expansion) y changes according to the recipe used, in particular if the DE takes part or not into the virialization process. Whatever is the correct formulation for the virialization process in clustering DE models, our ignorance on the exact value of y will not qualitatively affect our discussion and conclusions; therefore, for simplicity we will use $y = 1/2$, as in the EdS model (see also the discussion in Batista & Pace 2013). Since clustering DE does not alter the temporal evolution of the DM energy density parameter, we can still write $\Delta_{\mathrm{V}} = \zeta(x/y)^3$, where ζ represents the non-linear overdensity at turnaround and x is the scale factor normalized at the turnaround scale factor. Our results for the (non-)rotating case are presented in Figs 4 and 5.

As before, we limit ourselves to the study of the effects of the shear and rotation terms at galactic scales, since this is the mass scale where the effect is stronger. As for the δ_c parameter, also in this case the DE models differ mostly from the reference model when the effective sound speed is of the order unity, while for $c_{\mathrm{eff}}^2 = 0$ the models are closer to the ΛCDM model. We also notice that, since at high redshifts the amount of DE is negligible, DE models recover the ΛCDM model. The model differing more is, once again, the DE5 with $c_{\mathrm{eff}}^2 = 1$ (see Fig. 2). Quintessence (phantom) models have lower (higher) values of Δ_{V} with respect to the ΛCDM model. These results are qualitatively similar to what found in Pace et al. (2010). Model DE7 behaves like the quintessence models having slightly smaller values for the case $c_{\mathrm{eff}}^2 = 0$.
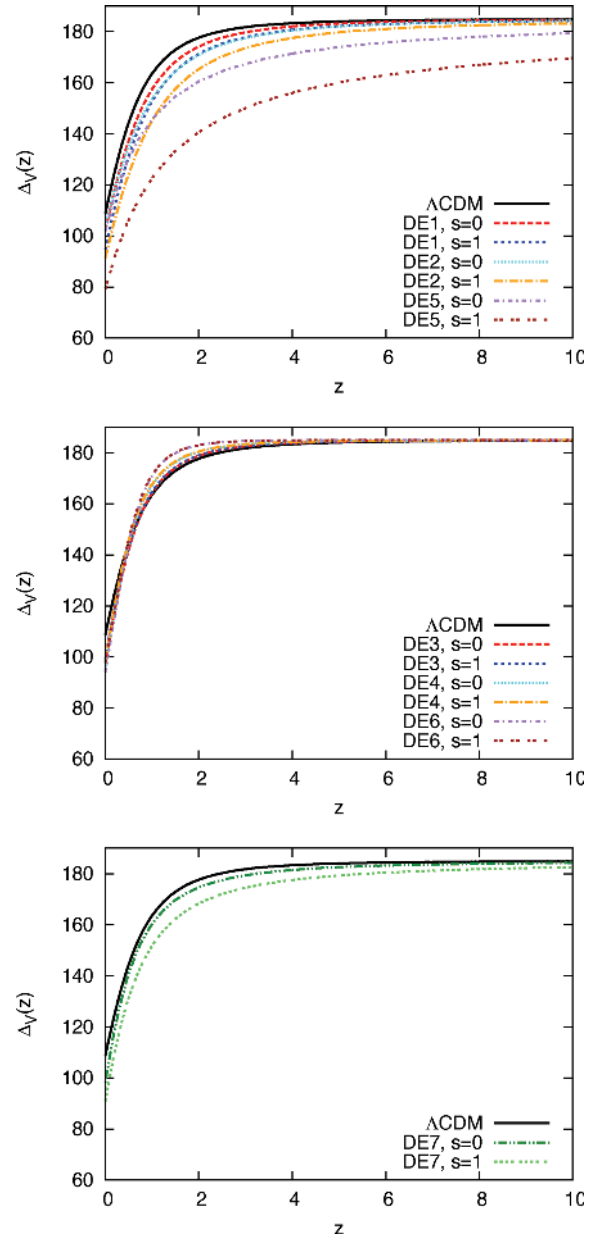
We find qualitatively similar results in the ESCM (see Fig. 5). With respect to the usual case, we observe, as expected, that the virial overdensity is higher than for the usual SCM but the ΛCDM model is recovered at high redshifts. Once again major differences take place when $c_{\mathrm{eff}}^2 = 1$. We notice that our results are similar to what was found in Del Popolo et al. (2013c).
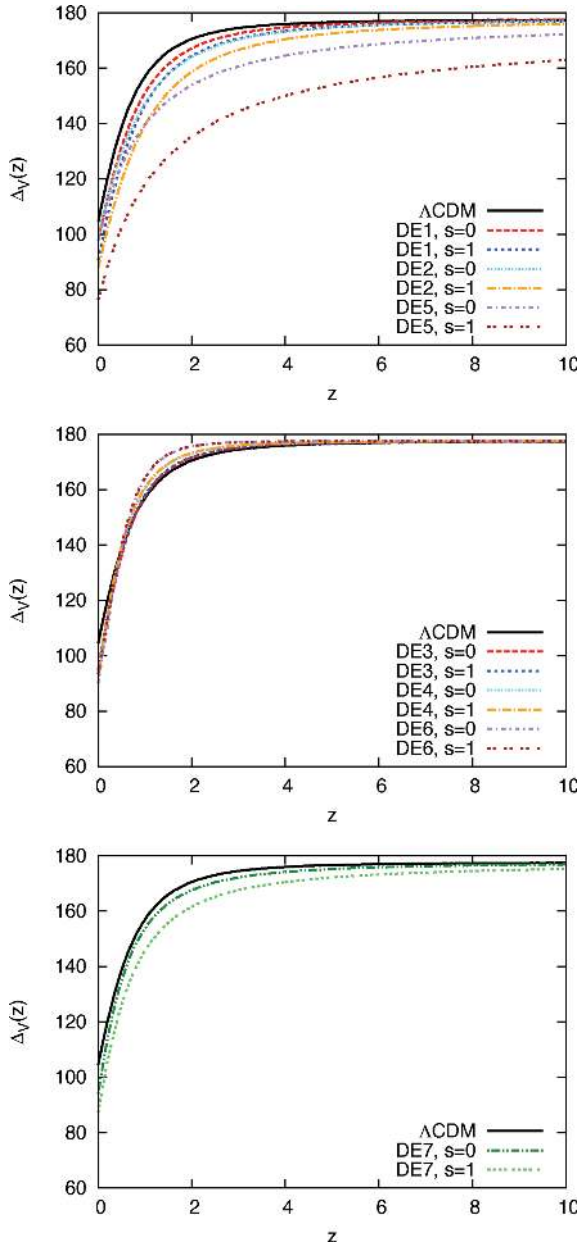
Figure 4. Virial overdensity for the difference DE models. In the upper (middle) panel, we show results for the quintessence (phantom) models while in the bottom panel, we present results for the model with barrier crossing. Line styles and colours are as in Fig. 2.

Figure 5. Virial overdensity for the difference DE models with shear and rotation terms included. In the upper (middle) panel, we show results for the quintessence (phantom) models while in the bottom panel, we present results for the model with barrier crossing. Panels refer to galactic-scale mass objects ($M \approx 10^{11}\,M_\odot\,h^{-1}$), corresponding to $\alpha = 0.05$. Line styles and colours are as in Fig. 2.

We can therefore conclude that clustering DE models behave qualitatively as non-clustering DE models in both the SCM and ESCM. Shear and rotation terms only oppose the collapse, without modifying it.

As said before, we have made the assumption that the shear and the rotation terms affect only DM. We performed a similar analysis relaxing this assumption and supposing that both DM and DE are influenced by these additional non-linear terms, and then using a single equation for the velocity field, equation (25). The results obtained are very similar to what presented here; therefore, in the following, we will assume that DM and DE have a different peculiar velocity.

4.2 Mass function

Here we study the effect of the shear and rotation terms on the number counts of haloes. We assume that the analytical formulation by Sheth and Tormen (Sheth & Tormen 1999, 2002; Sheth et al. 2001) is valid also for clustering DE models without any modification (but see also Del Popolo & Gambera 1999; Del Popolo 2006). The mass function critically depends on the linear overdensity parameter δ_c, the growth factor and on the linear power spectrum normalization σ_8. To properly evaluate the effects of the extra terms in the SCM formalism, we assume that all the models have the same σ_8 at $z = 0$ and to highlight the effect, we consider the number of objects at $z = 0$ and 1 above a given mass M of the halo. We will
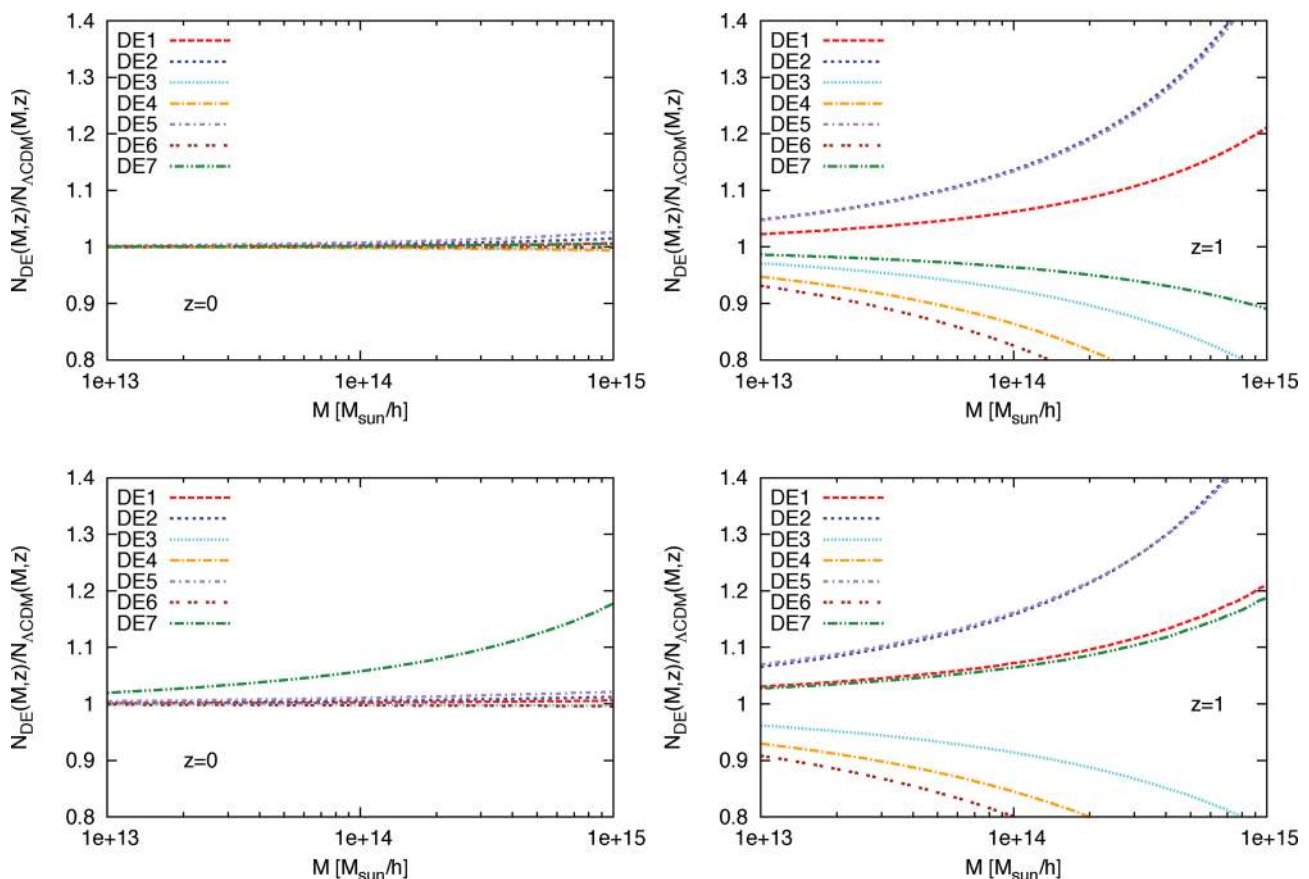
Figure 6. Ratio of the number of objects above a given mass M for haloes at $z = 0$ (left-hand panels) and $z = 1$ (right-hand panels) between the DE models and the ΛCDM model. The upper panels show ratios for the usual SCM while the bottom panels ratios for the ESCM. The red dashed curve represents the DE1 model, the blue short-dashed curve the DE2 model, the cyan dotted curve the DE3 model, the yellow dot–dashed curve the DE4 model, the violet dotted short-dashed curve the DE5 model, the brown dot-dotted curve the DE6 model and the green dashed dot-dotted curve the DE7 model.

assume as transfer function for the linear matter power spectrum the functional form given by Bardeen et al. (1986) and $\sigma_8 = 0.776$ as normalization of the power spectrum, in agreement with the most recent measurements (Planck Collaboration 2013b,e).

A comment is necessary at this point to explain the choice of the matter power spectrum normalization. In Batista & Pace (2013) and Del Popolo et al. (2013c), we had a different normalization for each model, such that all the models would have the same amplitude of perturbations at the CMB epoch ($z \approx 1100$). Here, instead we enforce all the models to share the same normalization today. While a model-dependent normalization should be in general preferred, here we want to isolate the effect of the shear and rotation terms and analyse their behaviour. If we would also have a different σ_8 for each model, a direct comparison between them would be more difficult.

In Fig. 6, we show the ratio of the number of objects above a given mass M between the DE models and the ΛCDM model, restricting the analysis to the case $c_{\rm eff}^2 = 0$. In the upper (lower) panel, we present results without (with) rotation and shear terms. Left-hand (right-hand) panels are for haloes at $z = 0$ ($z = 1$). As expected, since the models have the same normalization of the matter power spectrum, at $z = 0$ the models have essentially the same number of objects, with very small differences for masses $M \approx 10^{15}$. In particular, quintessence models (DE1, DE2, DE5) show a slight excess of structures, while phantom models (DE3, DE4, DE6) show a decrement in the number of structures. Model DE7 is at all effects

identical to model DE1. Differences grow with redshift and at $z = 1$, they can be few tens of per cent, keeping though the same qualitative behaviour. Models with highest differences are those with the equation-of-state parameter differing mostly from $w = -1$. Interestingly enough, model DE7 shows now a decrement of $\simeq 10$ per cent with respect to the ΛCDM model. With the inclusion of the shear and rotation terms, we see a behaviour qualitatively similar to the standard case, with major differences at higher redshifts (due to the time evolution of the DE), but with a smaller number of objects, at the level of per cent for the phantom models, while quintessence models are largely unaffected. Results are consistent with the time evolution of the linear overdensity factor δ_c (see Figs 2 and 3). The case of model DE7 is interesting, which shows a very strong dependence on the inclusion of the non-linear terms already at very low redshifts, but its time dependence is very weak. This is probably due to the change of regime between the phantom and the quintessence one. Note that ratios shown in the second row are taken with respect to the ΛCDM model evaluated in the ESCM.

DE models with $c_{\rm eff}^2 = 1$ (see also Del Popolo et al. 2013b) deserve a comment. Due to the major differences between the linear overdensity parameter δ_c of these models with respect to the ΛCDM one, we expect differences already at $z = 0$ and they increase in value at $z = 1$. Qualitatively, the same behaviour is nevertheless recovered, so models DE3, DE4 and DE6 (phantom models) show a decrement in the number of objects. Analogously to the case with $c_{\rm eff}^2 = 0$, the two additional non-linear terms just slightly increase

differences with respect to the standard case, in agreement with Figs 2 and 3.

As explained before in Section 4.1, the linear overdensity parameter δ_c becomes mass dependent when shear and rotation are included. To evaluate the mass function when these additional non-linear terms are included, we therefore explicitly evaluate the contributions of the shear and rotation terms to δ_c for each mass, so as to have an exact evaluation of the mass function. This means that major differences will take place at small masses, while at cluster scales differences between the two different mass functions will be negligible. This is indeed the case in the lower panels of Fig. 6, with the exceptions of model DE7 as clarified above.

After establishing the effect of the shear and rotation terms on the mass function, we investigate deeper the effects of the clustering of the DE fluid. In this case, the total mass of the halo is affected by DE perturbations (Creminelli et al. 2010; Basse et al. 2011; Batista & Pace 2013), and we need to take this into account evaluating the fraction of the halo mass given by the clustering of the DE. How and how much DE contributes to the halo mass depends on the virialization process, in particular whether DE virializes and on which time-scale. If the halo mass is modified, then the merging history (see e.g. Lacey & Cole 1993) must also reflect somehow this additional contribution. According to the equation-of-state parameter, DE can add or subtract mass to the total halo mass. An exact treatment of this problem must take into account the nature of the DE fluid and its exact virialization process. This is beyond the purpose of this work and we will use an approximate recipe, limiting ourselves to the case in which $c_{\text{eff}}^2 = 0$ and we will assume that DE virializes with DM on the same time-scale (see Batista & Pace 2013). In the following, we will describe how to evaluate the fraction of DE with respect to the total mass of the halo (Batista & Pace 2013).

As done in Section 4.1, we will assume that $y = R_{\text{vir}}/R_{\text{ta}} = 1/2$ as in the EdS universe. For this model, the virial overdensity Δ_{V} can be evaluated analytically, and in the literature two different definitions are usually adopted. The most common one (Wang & Steinhardt 1998) evaluates it at the collapse redshift z_c: $\Delta_{\text{V}}(z_c) = \rho_{\text{m}}(z_v)/\bar{\rho}_{\text{m}}(z_c) \simeq 178$, where z_v is the virialization redshift. According to Lee & Ng (2010) and Meyer, Pace & Bartelmann (2012), it is more correct to evaluate it at the virialization redshift: $\Delta_{\text{V}}(z_v) = \rho_{\text{m}}(z_v)/\bar{\rho}_{\text{m}}(z_v) \simeq 147$. These values will obviously change in the presence of DE and they depend on the properties of DE (Lahav et al. 1991; Maor & Lahav 2005; Creminelli et al. 2010; Basse et al. 2011).

The fraction ($\epsilon(z)$) of DE mass (M_{DE}) with respect to the DM mass (M_{DM}) is

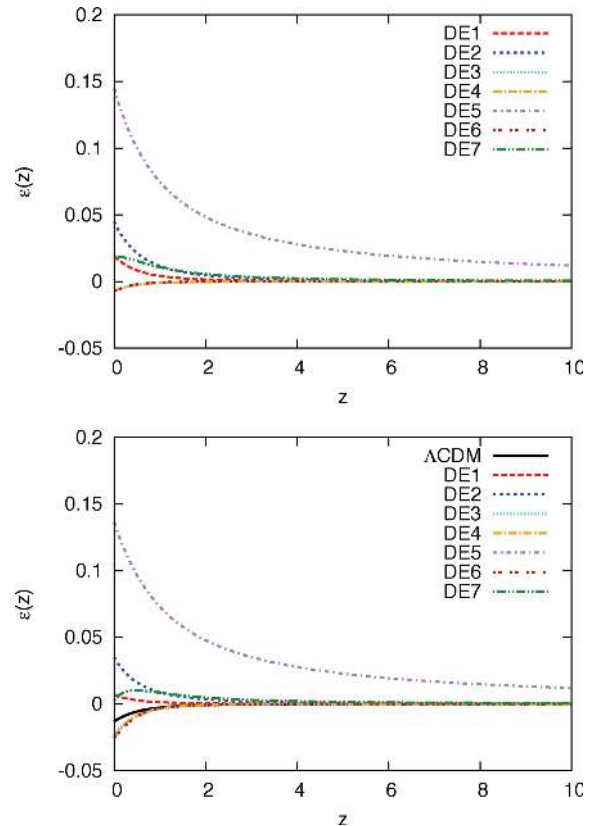$$\epsilon(z) = \frac{M_{\text{DE}}}{M_{\text{DM}}} . \qquad (26)$$

We define the DM mass as

$$M_{\text{DM}} = 4\pi \int_0^{R_{\text{vir}}} dR\, R^2 (\bar{\rho}_{\text{DM}} + \delta\rho_{\text{DM}}) , \qquad (27)$$

and the DE mass as

$$M_{\text{DE}_{\text{P}}} = 4\pi \int_0^{R_{\text{vir}}} dR\, R^2 \delta\rho_{\text{DE}} (1 + 3c_{\text{eff}}^2) . \qquad (28)$$

We label the DE mass as $M_{\text{DE}_{\text{P}}}$ (see equation 28) to indicate that in its definition we consider only the contribution coming from the perturbation.

Figure 7. Fraction of the DE mass with respect to the DM mass according to the definition of equations (28) (upper panel) and (29) (lower panel). The black solid curve shows the ΛCDM model, the red dashed curve the DE1 model, the blue short-dashed curve the DE2 model, the cyan dotted curve the DE3 model, the yellow dot–dashed curve the DE4 model, the violet dotted short-dashed curve the DE5 model, the brown dot-dotted curve the DE6 model and the green dashed dot-dotted curve the DE7 model.

If instead we also consider the background contribution, the mass definition becomes

$$M_{\text{DE}_{\text{T}}} = 4\pi \int_0^{R_{\text{vir}}} dR\, R^2 \left[(1 + 3w)\bar{\rho}_{\text{DE}} + (1 + 3c_{\text{eff}}^2)\delta\rho_{\text{DE}} \right] , \qquad (29)$$

in analogy with the Poisson equation. In this case, there will also be a contribution for the ΛCDM model. However, since the background term varies in time, regardless of the halo formation history, this contribution is not constant and should be interpreted just as a crude estimate of the background DE energy to the halo mass.

In Fig. 7, we show the fraction of the DE mass with respect to the DM mass according to the definition used in equations (28) (upper panel) and (29) (lower panel) for the case $c_{\text{eff}}^2 = 0$ only in the standard SCM. For a deeper discussion on the mass definition adopted, see Batista & Pace (2013). We just show results for the standard SCM since rotation and shear have a negligible effect on $\epsilon(z)$. In particular for quintessence models, the extra terms slightly reduce the DE contribution, while for the phantom models, $\epsilon(z)$ being negative and therefore subtracting mass to the halo, this function is slightly higher, or in absolute values, again slightly smaller. The same result is obtained for the barrier-crossing model. The effect of the shear and rotation terms is of the order of tenth of per cent.

As expected (see Fig. 7), quintessence models give a positive contribution to the total mass of the halo while phantom models subtract mass. Differences are of the order of the per cent level, except for model DE5, where differences are up to ≈ 14 per cent. In
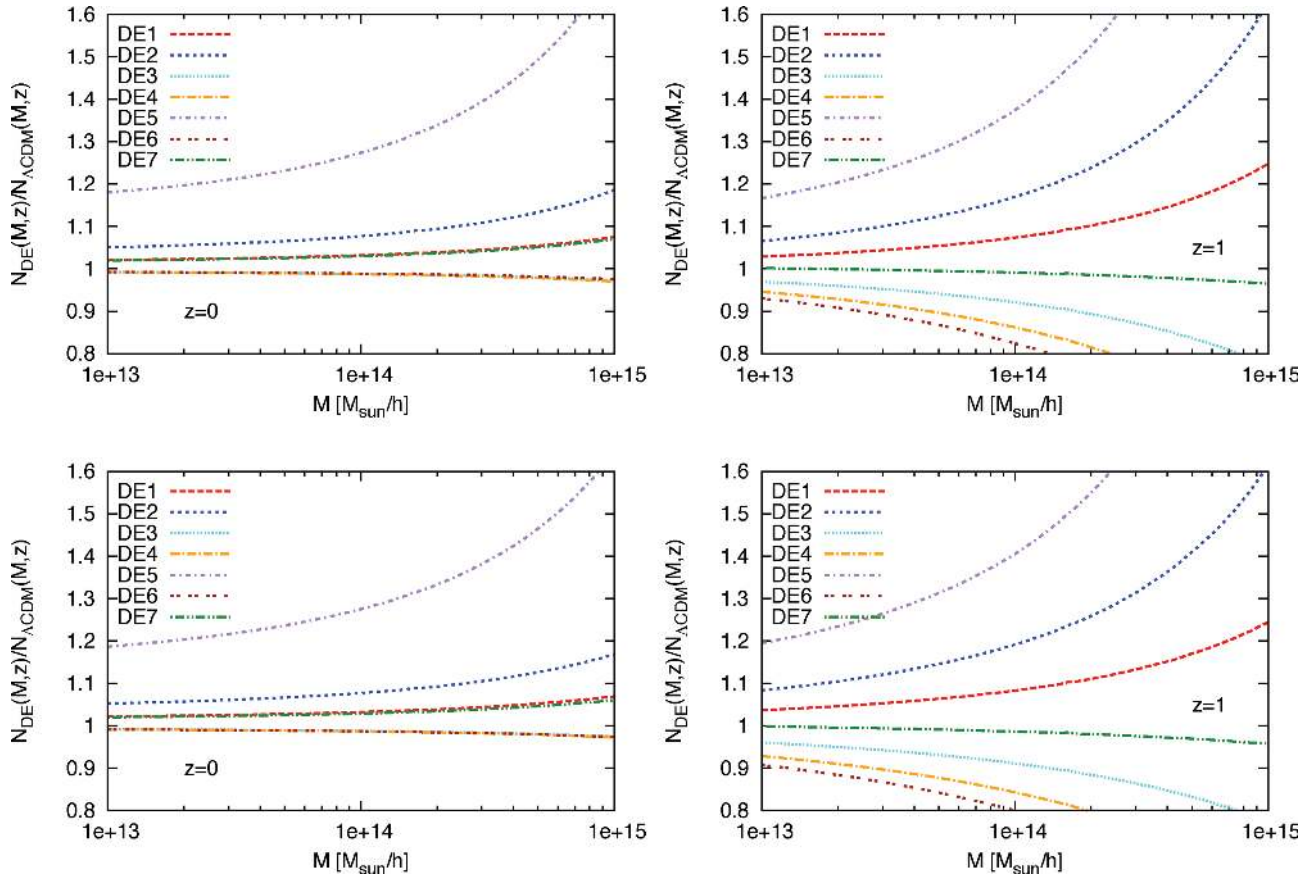
Figure 8. Ratio of the number of objects above a given mass M for haloes at $z = 0$ (left-hand panels) and $z = 1$ (right-hand panels) between the DE models and the ΛCDM model, using the mass definition in equation (28). The upper panels show ratios for the usual SCM while the bottom panels show the ratios for the ESCM. Line styles and colours are as in Fig. 6.

agreement with Batista & Pace (2013), we also notice that the mass correction evaluated with equation (29) is smaller than when only perturbations are taken into account. Major differences are at $z = 0$ and become null at higher redshifts. This is expected, since $\epsilon(z)$ is significantly different from zero at low redshifts. Exception is once again model DE5. This is due to the fact that its equation of state is very different from $w = -1$. The inclusion of a mass correction term will affect the mass function and major differences will take place for $z \approx 0$, as we show in Fig. 8. Differences are again more pronounced for high masses where they can be up to 20 per cent while for low masses they are only of the order of 5 per cent at most. The hierarchy of the models, i.e. how much they are affected, directly reflects the values of the mass correction.

In Fig. 8, we show the ratio of the mass function with the new mass definition, $M(1 - \epsilon)$, where ϵ is given by equation (26). Since we only consider the contribution of the DE perturbations, the cosmological constant does not contribute to the total mass of the system. Quintessence (phantom) models have a lower (higher) number of objects at the low-mass end of the mass function and a higher (lower) number of objects at the high-mass tail. This can be easily explained by taking into account the relative contribution of the DE component to the total mass of the halo (see the upper panel of Fig. 7). A positive (negative) contribution to the total mass shifts the mass function towards lower (higher) values and, as consequence, we obtain a higher (lower) number of objects. At the high-mass end, the contribution of the linear overdensity parameter

δ_c dominates, giving the opposite trend with respect to the low-mass tail.

We can conclude that shear and rotation terms have in general a negligible contribution also when the mass definition in equation (28) is adopted.

Similar results apply for the case $c_{\rm eff} = 1$, where we note that since perturbations in DE are negligible, so is the mass correction.

5 CONCLUSIONS

In this work, we studied the effect of the inclusion of the term $\sigma^2 - \omega^2$. We analysed its impact in the framework of the SCM and in particular on the linear overdensity parameter δ_c and on the virial overdensity Δ_V. The parameter δ_c is one of the ingredients of the mass function, and its variation reflects on the mass function and, as consequence, on the number of objects at a given redshift.

We consider DM and DE component as two fluids described by the respective equation of state and both of them can cluster. In particular, we relate the pressure perturbations to density perturbations for the DE component with the effective sound speed parameter $c_{\rm eff}^2$, which we assume to be constant and its values were fixed to $c_{\rm eff}^2 = 0$ and 1, as currently done in the literature.

The $\sigma^2 - \omega^2$ term, being non-linear, appears only in the non-linear equation describing the evolution of the peculiar velocity; therefore, the growth factor is not affected. We made the assumption that only DM is affected by this additional non-linear term, but if

we instead suppose that both DM and DE experience shear and rotation, we showed that results are largely unaffected, since for the models studied DE perturbations are subdominant.

We showed that the additional non-linear term opposes the collapse, as for the case in which the DE is only at the background level. Opposing the collapse, it makes such that both δ_c and Δ_V have a higher value with respect to the standard SCM. Increments in the linear overdensity parameter are of the order of 40 per cent for low masses, analogously to what found in Del Popolo et al. (2013c), where the ESCM was studied in non-clustering DE models. Quintessence models have always a lower value of δ_c, both in the standard and in the ESCM. Phantom models instead present higher values, due to the faster expansion of the universe. A similar behaviour is found for the virial overdensity parameter Δ_V.

Differences in the SCM parameters reflect obviously in the mass function and in particular in the number of objects above a given mass (see Section 4.2). To properly evaluate the effect of the additional term, we use the same normalization of the linear matter power spectrum for all the models. Moreover, considering the number of objects above a given mass does not introduce any geometrical dependence on the results that will therefore depend only on the particular model considered (DE equation-of-state parameter and effective sound speed). Comparing results in the ESCM with the standard SCM, we notice that the differences are in general small, of the order of the per cent for all the models considered in this work.

When DE clusters, following Batista & Pace (2013), we speculate that the halo mass can be modified by the inclusion of the DE perturbation into its definition. We therefore evaluate the correction to the halo mass and we found that this is generally of the order of few per cent at low mass (but higher on cluster scales) and its sign (being positive or negative) depends on the equation of state of the DE component. The shear and rotation terms slightly modify this function, making it closer to zero when these terms are taken into account. Due to the small value of this correction factor, modifications in the number of objects are also small.

We can therefore conclude that effects of rotations in clustering DE models are modest and comparable to what found in Del Popolo et al. (2013a,c) for non-clustering DE models. Hence, we may also expect that the effect of clustering DE in more realistic models of structure formation can be well described by the usual SCM.

ACKNOWLEDGEMENTS

REFERENCES

Abramo L. R., Batista R. C., Liberato L., Rosenfeld R., 2007, J. Cosmol. Astro-Part. Phys., 11, 12
Abramo L. R., Batista R. C., Liberato L., Rosenfeld R., 2008, Phys. Rev. D, 77, 067301
Abramo L. R., Batista R. C., Rosenfeld R., 2009a, J. Cosmol. Astropart. Phys., 7, 40
Abramo L. R., Batista R. C., Liberato L., Rosenfeld R., 2009b, Phys. Rev. D, 79, 023516
Alcaniz J. S., Lima J. A. S., Cunha J. V., 2003, MNRAS, 340, L39
Allen S. W., Schmidt R. W., Ebeling H., Fabian A. C., van Speybroeck L., 2004, MNRAS, 353, 457
Allen S. W., Rapetti D. A., Schmidt R. W., Ebeling H., Morris R. G., Fabian A. C., 2008, MNRAS, 383, 879
Amanullah R. et al., 2010, ApJ, 716, 712
Armendariz-Picon C., Mukhanov V., Steinhardt P. J., 2001, Phys. Rev. D, 63, 103510
Ascasibar Y., Yepes G., Gottlöber S., Müller V., 2004, MNRAS, 352, 1109
Astashenok A. V., del Popolo A., 2012, Classical Quantum Gravity, 29, 085014
Astier P. et al., 2006, A&A, 447, 31
Avila-Reese V., Firmani C., Hernández X., 1998, ApJ, 505, 37
Bardeen J. M., Bond J. R., Kaiser N., Szalay A. S., 1986, ApJ, 304, 15
Basilakos S., Sanchez J. C. B., Perivolaropoulos L., 2009, Phys. Rev. D, 80, 043530
Basilakos S., Plionis M., Solà J., 2010, Phys. Rev. D, 82, 083512
Basse T., Eggers Bjælde O., Wong Y. Y. Y., 2011, J. Cosmol. Astropart. Phys., 10, 38
Batista R. C., Pace F., 2013, J. Cosmol. Astropart. Phys., 6, 44
Bernardeau F., 1994, ApJ, 433, 1
Bertschinger E., 1985, ApJS, 58, 39
Bett P., Eke V., Frenk C. S., Jenkins A., Helly J., Navarro J., 2007, MNRAS, 376, 215
Blake C. et al., 2011, MNRAS, 415, 2876
Casaponsa B., Bridges M., Curto A., Barreiro R. B., Hobson M. P., Martínez-González E., 2011, MNRAS, 416, 457
Chevallier M., Polarski D., 2001, Int. J. Mod. Phys. D, 10, 213
Chimento L. P., Lazkoz R., 2005, Phys. Rev. D, 71, 023505
Cole S. et al., 2005, MNRAS, 362, 505
Creminelli P., D'Amico G., Noreña J., Vernizzi F., 2009, J. Cosmol. Astropart. Phys., 2, 18
Creminelli P., D'Amico G., Noreña J., Senatore L., Vernizzi F., 2010, J. Cosmol. Astropart. Phys., 3, 27
Curto A., Martínez-González E., Barreiro R. B., Hobson M. P., 2011, MNRAS, 417, 488
Del Popolo A., 2002, A&A, 387, 759
Del Popolo A., 2006, A&A, 448, 439
Del Popolo A., 2007, Astron. Rep., 51, 169
Del Popolo A., 2014, Int. J. Mod. Phys. D, 23, 1430005
Del Popolo A., Gambera M., 1999, A&A, 344, 17
Del Popolo A., Ercan E. N., Xia Z., 2001, AJ, 122, 487
Del Popolo A., Pace F., Lima J. A. S., 2013a, Int. J. Mod. Phys. D, 22, 50038
Del Popolo A., Pace F., Maydanyuk S. P., Lima J. A. S., Jesus J. F., 2013b, Phys. Rev. D, 87, 043527
Del Popolo A., Pace F., Lima J. A. S., 2013c, MNRAS, 430, 628
Dotter A., Sarajedini A., Anderson J., 2011, ApJ, 738, 74
Eisenstein D. J. et al., 2005, ApJ, 633, 560
Ferreira P. G., Joyce M., 1998, Phys. Rev. D, 58, 023503
Fillmore J. A., Goldreich P., 1984, ApJ, 281, 1
Giannantonio T., Scranton R., Crittenden R. G., Nichol R. C., Boughn S. P., Myers A. D., Richards G. T., 2008, Phys. Rev. D, 77, 123520
Gunn J. E., Gott J. R., III, 1972, ApJ, 176, 1
Gurevich A. V., Zybin K. P., 1988a, Zh. Eksp. Teor. Fiz., 94, 3
Gurevich A. V., Zybin K. P., 1988b, Zh. Eksp. Teor. Fiz., 94, 5
Guth A. H., 1981, Phys. Rev. D, 23, 347
Haiman Z., Mohr J. J., Holder G. P., 2001, ApJ, 553, 545
Hinshaw G. et al., 2013, ApJS, 208, 19
Hiotelis N., del Popolo A., 2013, MNRAS, 436, 163
Ho S., Hirata C., Padmanabhan N., Seljak U., Bahcall N., 2008, Phys. Rev. D, 78, 043519
Hoekstra H., Mellier Y., van Waerbeke L., Semboloni E., Fu L., Hudson M. J., Parker L. C., Tereno I., Benabed K., 2006, ApJ, 647, 116
Hoffman Y., 1986, ApJ, 308, 493
Hoffman Y., 1989, ApJ, 340, 69
Hoffman Y., Shaham J., 1985, ApJ, 297, 16
Jarosik N. et al., 2011, ApJS, 192, 14
Jarvis M., Jain B., Bernstein G., Dolney D., 2006, ApJ, 644, 71
Knop R. A. et al., 2003, ApJ, 598, 102
Komatsu E., 2010, Classical Quantum Gravity, 27, 124010
Komatsu E. et al., 2011, ApJS, 192, 18

Krauss L. M., Chaboyer B., 2003, Science, 299, 65
Lacey C., Cole S., 1993, MNRAS, 262, 627
Lahav O., Lilje P. B., Primack J. R., Rees M. J., 1991, MNRAS, 251, 128
Lee S., Ng K.-W., 2010, J. Cosmol. Astropart. Phys., 10, 28
Lim E. A., Sawicki I., Vikman A., 2010, J. Cosmol. Astropart. Phys., 5, 12
Linde A., 1990, Phys. Lett. B, 238, 160
Linder E. V., 2003, Phys. Rev. Lett., 90, 091301
Maor I., Lahav O., 2005, J. Cosmol. Astropart. Phys., 7, 3
Meyer S., Pace F., Bartelmann M., 2012, Phys. Rev. D, 86, 103002
Mota D. F., van de Bruck C., 2004, A&A, 421, 71
Novosyadlyj B., Sergijenko O., Durrer R., Pelykh V., 2012, Phys. Rev. D, 86, 083008
Nunes N. J., Mota D. F., 2006, MNRAS, 368, 751
Ohta Y., Kayo I., Taruya A., 2003, ApJ, 589, 1
Ohta Y., Kayo I., Taruya A., 2004, ApJ, 608, 647
Pace F., Waizmann J.-C., Bartelmann M., 2010, MNRAS, 406, 1865
Pace F., Fedeli C., Moscardini L., Bartelmann M., 2012, MNRAS, 422, 1186
Pace F., Moscardini L., Crittenden R., Bartelmann M., Pettorino V., 2014, MNRAS, 437, 547
Percival W. J. et al., 2010, MNRAS, 401, 2148
Perlmutter S. et al., 1999, ApJ, 517, 565
Pettorino V., Baccigalupi C., 2008, Phys. Rev. D, 77, 103003
Planck Collaboration, 2013a, preprint (arXiv:1303.5075)
Planck Collaboration, 2013b, preprint (arXiv:1303.5076)
Planck Collaboration, 2013c, preprint (arXiv:1303.5079)
Planck Collaboration, 2013d, preprint (arXiv:1303.5086)
Planck Collaboration, 2013e, preprint (arXiv:1303.5080)
Press W. H., Schechter P., 1974, ApJ, 187, 425
Reid B. A. et al., 2010, MNRAS, 404, 60
Rest A. et al., 2013, preprint (arXiv:1310.3828)

Riess A. G. et al., 1998, AJ, 116, 1009
Riess A. G. et al., 2004, ApJ, 607, 665
Riess A. G. et al., 2007, ApJ, 659, 98
Ryden B. S., Gunn J. E., 1987, ApJ, 318, 15
Scolnic D. et al., 2013, preprint (arXiv:1310.3824)
Shafer D. L., Huterer D., 2014, Phys. Rev. D, 89, 063510
Shaw L. D., Weller J., Ostriker J. P., Bode P., 2006, ApJ, 646, 815
Sheth R. K., Tormen G., 1999, MNRAS, 308, 119
Sheth R. K., Tormen G., 2002, MNRAS, 329, 61
Sheth R. K., Mo H. J., Tormen G., 2001, MNRAS, 323, 1
Sievers J. L. et al., 2013, J. Cosmol. Astropart. Phys., 10, 60
Starobinsky A. A., 1980, Phys. Lett. B, 91, 99
Subramanian K., Cen R., Ostriker J. P., 2000, ApJ, 538, 528
Tarrant E. R. M., van de Bruck C., Copeland E. J., Green A. M., 2012, Phys. Rev. D, 85, 023503
Tegmark M. et al., 2004a, Phys. Rev. D, 69, 103501
Tegmark M. et al., 2004b, ApJ, 606, 702
Tonry J. L. et al., 2003, ApJ, 594, 1
Vikhlinin A. et al., 2009, ApJ, 692, 1060
Wang L., Steinhardt P. J., 1998, ApJ, 508, 483
Wang S., Khoury J., Haiman Z., May M., 2004, Phys. Rev. D, 70, 123008
Williams L. L. R., Babul A., Dalcanton J. J., 2004, ApJ, 604, 18
Wintergerst N., Pettorino V., 2010, Phys. Rev. D, 82, 103516
Zaroubi S., Hoffman Y., 1993, ApJ, 416, 410

This paper has been typeset from a TEX/LATEX file prepared by the author.